magnetochemistry

MDPI

Article

Magnetic Anisotropy Vectors and Mixing of Spin-States Across Spin Transition in $[Mn^{III}(pyrol)_3(tren)]$ Explored with Polarized Neutron Diffraction

Pikesh Pal [1], Iurii Kibalin [2], Arsen Goukassov [1], Thomas C. Hansen [3], Eddy Lelièvre-Berna [3], Yann Garcia [4] and Grégory Chaboussant [1,*]

[1] Laboratoire Léon Brillouin, UMR12 CNRS-CEA, Université Paris-Saclay, CEA Saclay, 91191 Gif-sur-Yvette, France; pikesh.pal@cea.fr (P.P.); arsen.goukassov@cea.fr (A.G.)
[2] European Spallation Source ERIC, P.O. Box 176, SE-221 00 Lund, Sweden; iurii.kibalin@ess.eu
[3] Institut Laue—Langevin (ILL), 71, Avenue des Martyrs, 38042 Grenoble Cedex 9, France; hansen@ill.eu (T.C.H.); lelievre@ill.eu (E.L.-B.)
[4] Institute of Condensed Matter and Nanosciences, Molecular Chemistry, Materials and Catalysis (IMCN/MOST), Université Catholique de Louvain, Place Pasteur 1, bte L4.01.03, 1348 Louvain-la-Neuve, Belgium; yann.garcia@uclouvain.be
* Correspondence: gregory.chaboussant@cea.fr

Abstract

$[Mn^{III}(pyrol)_3(tren)]$ {$(Hpyrol)_3$tren = tris(1-(2-azolyl)-2-azabuten-4-yl)amine)} is a mononuclear spin-transition compound switching between high spin (HS, S = 2) and low spin (LS, effective S = 1) around 47 K, preserving $I\bar{4}3d$ symmetry. Its magnetic anisotropy is studied by calculating the atomic susceptibility tensor from the refinement of polarized neutron powder diffraction. The analysis reveals that the weakly prolate-type atomic magnetic anisotropy in the HS state abruptly switches to uniaxial needle-shaped/Ising-type anisotropy in the LS state. However, the overall magnetic anisotropy of the unit cell remains isotropic due to the cubic nature of the crystal symmetry. Irreversible coexistence of mixed spin states HS/LS is observed in the vicinity of the cooperative spin crossover, where the average magnetic moment of Mn^{3+} shows a hysteretic temperature variation. This hysteretic mixing of HS and LS at intermediate temperatures suggests complex growth and nucleation of HS and LS domains. The study demonstrates that polarized powder neutron diffraction is a unique and powerful tool for describing complex magnetic anisotropies and magneto-structural correlations in molecular-based magnetic materials.

Keywords: molecular magnetism; polarized neutron diffraction; spin-transition; magnetic anisotropy; zero-field splitting; spin-state mixing

Academic Editor: Marius Andruh

Received: 16 March 2026
Revised: 18 April 2026
Accepted: 6 May 2026
Published: 12 May 2026

1. Introduction

Magnetic anisotropy plays a crucial role in determining the electronic energy landscape, the relaxation barrier, and magnetic tunneling in non-interacting or interacting magnetic centers of so-called molecular magnets, a large class of materials that have promising potential for spintronics and quantum computing [1–3]. It links the structural symmetry of the coordination environment to the directional magnetic response, i.e., the easy or hard axis of the magnetic center under an applied magnetic field [1]. Depending on the nature of the correlations between spins and the symmetry of the coordination environment, magnetic anisotropy can also play an important role in defining the coupling

occurring between spin and charge degrees of freedom in molecular-based magnetoelectric (ME) materials [4]. In spin crossover (SCO) and spin-transition molecular systems, the magnetic anisotropy changes significantly, driven by the subtle balance between the electrostatic field on the magnetic ion and the spin-pairing energy, under the influence of external controllable perturbations such as temperature, light, magnetic field, or pressure [5]. Therefore, understanding magnetic anisotropy and magneto-structural correlation in SCO materials is necessary to make progress towards potential applications.

Polarized Neutron Diffraction (PND) on single crystals analyzed using the susceptibility tensor approach [6,7] has proven to be a unique and powerful technique to measure anisotropy among other commonly practiced methods, which are Electron Paramagnetic Resonance (EPR), magnetometry (SQUID, VSM, and torque), and Inelastic Neutron Scattering (INS). It is known that EPR provides anisotropy information limited to the magnitude and sign of the magnetic anisotropic parameters (axial D and rhombic E terms) and g tensors when there is one molecular orientation per unit cell. However, for compounds with binuclear or multinuclear orientations, this technique has limitations in determining individual g and D anisotropy tensors. Single-crystal magnetometry can provide anisotropy information by measuring the susceptibility tensor in reference to crystal axes that, in general, do not coincide with the molecular symmetry axis, since the magnetic anisotropy in molecular magnets is the combination of molecular anisotropy and crystal symmetry of the space group. Alternatively, INS provides a direct scalar measurement of zero-field splitting (ZFS) anisotropy and crystal-field parameters by measuring zero-field excitation spectra. Recently, PND was developed to overcome the limitations of the earlier spin-density-distribution methods. Unlike earlier techniques, PND can explicitly measure the magnetic anisotropy tensor at sites with strong anisotropy (no collinearity between the induced magnetic moment and the applied field direction) [7]. The PND method is no longer restricted to single crystals; it has recently been extended to polycrystalline powder samples [8,9]. The integrated Rietveld refinement application platform CrysPy has been made available to refine the components of the susceptibility tensor from the flipping sum and difference intensities defined as $I_+ + I_-$ and $I_+ - I_-$. Here, I_+ and I_- are the scattered intensities corresponding to the incident neutron polarization parallel and antiparallel to the applied field at the sample position, respectively. For polycrystalline samples, the sum and difference flipping intensities can be written as

$$I_+ + I_- \sim |N|^2 + |M_\perp|^2 \tag{1}$$

$$I_+ - I_- \sim N^* < \left(\vec{M}_\perp.\vec{P}\right) > + N < \vec{M}^*{}_\perp.\vec{P} > \tag{2}$$

where N is the nuclear structure factor and $\vec{M}_\perp\left(\vec{k}\right)$ is the component of the magnetic structure factor $\vec{M}\left(\vec{k}\right)$, perpendicular to the scattering vector $\vec{k}$. $\vec{P}$ is the polarization factor of the incident beam. The magnetic structure factor can be written as $\vec{M}\left(\vec{k}\right) = \sum_j \vec{m}_j f\left(\vec{k}\right)\exp\left(i\vec{k}.\vec{r}\right) = \sum_j \overleftrightarrow{\chi}_j \boldsymbol{H} f\left(\vec{k}\right)\exp\left(i\vec{k}.\vec{r}\right)$, where $\overleftrightarrow{\chi}_j$ is a symmetric second-rank tensor defined as

$$\begin{pmatrix} \chi_{11} & \chi_{12} & \chi_{13} \\ \chi_{12} & \chi_{22} & \chi_{23} \\ \chi_{13} & \chi_{23} & \chi_{33} \end{pmatrix} \tag{3}$$

χ_{ij} values are determined by the constraints of the site symmetry and obtained from the refinement of the sum and difference diffraction patterns (see Equations (1) and (2))

calculated from the measurement of I_+ and I_-. A more detailed mathematical formulation of PND can be found in Ref. [9].

In this paper, we present a Polarized Neutron Powder Diffraction (PNPD) study to determine the magnetic anisotropy vectors in the spin-transition compound $[Mn^{III}(pyrol)_3(tren)]$ in both its high-spin (HS) and low-spin (LS) states.

$[Mn^{III}(pyrol)_3(tren)]$ {(Hpyrol)$_3$tren = tris(1-(2-azolyl)-2-azabuten-4-yl)amine)} is a molecular complex in which Mn^{3+} undergoes an abrupt cooperative spin transition from HS ($S = 2$) to LS states (effective $S = 1$) at ~47 K [10–13], preserving its space group ($I\bar{4}3d$) [14]. The macroscopic magnetic susceptibility in the form of χT(T) is represented in Figure S8 of the Supplementary Information. The spin transition is evidenced by a sharp drop of χT characterized by a sizeable hysteresis (see the inset of Figure S8, Supplementary Information). In the HS state, the Mn^{3+} polyhedra possess dynamic Jahn–Teller (J-T) distortion [13,15–17]. Previous ESR [17] and the INS study [18] proposed that in the HS state, the Hamiltonian consists of uniaxial and rhombic terms (INS: $D = -5.73$ cm^{-1} and $|E| = 0.475$ cm^{-1}, respectively), which leads to effective axial anisotropy along the threefold symmetry axis through the Mn ion. In the LS state, the INS spectra suggest a large positive uniaxial ($D = 39.3$ cm^{-1}) term in the Hamiltonian under the influence of strong trigonal compression along the C_3 direction, which leads to an effective spin $S = 1$ [18]. J-T distortion in the HS state manifests electric dipoles that show paraelectric behavior [12,19]. These J-T dipoles are proposed to be coupled with the magnetic easy axis via spin–orbit coupling and provide a pathway for an enhanced second-order magnetoelectric (ME) coupling, which tends to align the local J-T distortion-generated dipoles. This experimentally observed and theoretically supported ME coupling raises the crucial importance of understanding the magnetic anisotropy with respect to the local molecular symmetry axis of the $[Mn^{III}(pyrol)_3(tren)]$ complex [16,19,20].

The present PNPD study monitors the magnetic anisotropy and magneto-structural correlations in both HS/LS states and across the spin transition. Our investigation elucidates the nature of the spin transition by examining the spin state during the thermal spin transition. Further, the study also demonstrates the capability of PNPD to map the magnetic anisotropy of molecular magnets in polycrystalline powder form.

2. Experiment Details

Neutron powder polarized diffraction was performed on the D20 powder diffractometer at the Institut Laue-Langevin (Grenoble, France) [21]. $[Mn^{III}(pyrol)_3(tren)]$ was prepared as a polycrystalline sample, adapting a procedure for the Fe^{III} analog [13]. A m = 0.8 g polycrystalline $[Mn^{III}(pyrol)_3(tren)]$ sample was tightly packed in a Vanadium sample holder and mounted in a cryomagnet. A 5.5 T vertical magnetic field was applied at the sample position. The neutron beam ($\lambda = 2.41$ Å) was polarized using a ^{3}He spin filter (built by DPT/SON team at the ILL) measuring 8 cm (width) × 10 cm (depth) × 22 cm (height), filled at 1.5 bar. The incident beam polarization was continuously monitored using two neutron beam monitors positioned before and after the filter, as described in [22]. The initial beam polarization exceeded 80%, and the filter was replaced daily to compensate for the decay of the ^{3}He polarization. The 10% depolarization induced by the sample was determined using a Heusler crystal placed before and after the sample. Flipping difference spectra were measured following the repeated sequence [+][−][−][+] to avoid integrating beam polarization variations into the data. Measurements were taken at 200 K and 5 K to probe the system significantly above and below the spin transition. Other measurements were taken in the vicinity of the transition between 44 K and 50 K. Temperature controllers were used to carefully set the temperature and avoid overshoots. Rietveld analysis was done using the CrysPy package [9] for refinement of the nuclear structure and molecular

susceptibility tensor. Bond, angular, and dihedral distortion parameters were estimated using the OctaDist package [23].

3. Results and Discussion

The flipping sum pattern at 200 K and 5.5 T is fitted to refine the structure ($I\bar{4}3d$). At this temperature and magnetic field, the signal-to-noise ratio in the observed difference pattern is very low; thus, it is not used for the refinement of the susceptibility tensor but rather for structural information (Suppl. Figure S1a,b). The fitted unit cell dimension is 20.087 Å, and the distorted MnN_6 coordination polyhedral (Suppl. Figure S2) exhibits two distinct bond lengths: Mn-N1 = 2.079 (3) Å and Mn-N2 = 2.151(5) Å, with a mean value of Mn-N bond length of 2.115 Å. The distortion of dynamically active J-T polyhedral MnN_6 is estimated by calculating ζ (), $\Sigma(^\circ)$, and Θ (°). The parameter ζ is the sum of deviations of metal-ligand bond lengths around the metal ion from the mean bond length. Σ is the parameter defined as the sum of the deviations from 90° of the *cis* angles in the coordination spheres so as to represent the angular deviation of the polyhedron from the ideal octahedron. The Θ parameter represents the trigonal or dihedral distortion and is defined as deviations from 60° of the 24 possible twist angles [23]. The distortion parameters at 200 K are ζ = 0.216 Å, Σ = 74.48°, and Θ = 242.70°. The significantly high value of Θ corresponds to the trigonal distortion as a consequence of twist around the C_3 axis passing through Mn^{3+}.

At lower temperatures, clear positive and negative peaks are visible in the flipping difference in the diffraction patterns, which are then fitted using the susceptibility tensor method. Background, shape parameters, asymmetry parameters, polarization factors, scale factors, and beam offset parameters are primarily refined for the flipping sum and are set to fixed values before the susceptibility tensor components are refined from the flipping difference patterns. Position of the Mn^{3+} ion is at the 16c site in $I\bar{4}3d$ space group symmetry, and thus the symmetry constraints apply to the refinable susceptibility components as $\chi_{11} = \chi_{22} = \chi_{33}$ and $\chi_{12} = \chi_{13} = \chi_{23}$. Therefore, two independent coordinates χ_{11} and χ_{12} of the matrix tensor are refined for all the patterns below 50 K. The fitted flipping sum and difference patterns are shown in the Supplementary Information (Suppl. Figures S3 and S4).

At 5 K, in the LS state, the refined values of these two independent components of the susceptibility tensor are χ_{11}= 0.0586(47) $\mu_B T^{-1}$ and χ_{12}= 0.043(14) $\mu_B T^{-1}$, and the corresponding eigenvalues are χ_1= 0.145 $\mu_B T^{-1}$, χ_2= χ_3 = 0.016 $\mu_B T^{-1}$. The anisotropy ellipsoid plotted over the molecule (Figure 1a) clearly indicates strong uniaxial Ising-type anisotropy with an easy magnetic axis oriented along four local <111> directions (Figure 1b), i.e., along the C_3 symmetry axis of the molecule. The strong axiality of the anisotropy ellipsoid can be realized by comparing the parallel and perpendicular components defined as $\chi_{\parallel} = \chi_{11} + 2\chi_{12} = \chi_1$ and $\chi_{\perp} = \chi_{11} - \chi_{12} = \chi_2 = \chi_3$ [9]. At 5 K, the component parallel to the C_3 axis is $\chi_{\parallel} = 0.145(49)\ \mu_B T^{-1}$ and the perpendicular component is $\chi_{\perp} = 0.0156(49)\ \mu_B T^{-1}$, which lies in the (111) plane. The ratio of these components ($\frac{\chi_{\parallel}}{\chi_{\perp}}$) is ~9.29(24), which signals a strong uniaxial nature of anisotropy in the LS state. At 5 K, while the unit cell parameter is a = 19.842(18) Å, values of the distortion parameters for MnN_6 are ζ = 0.339 Å, Σ = 53.302°, and Θ = 180.700°, and the average value of the Mn-N bond length is 2.0283 Å. The distortion values clearly show that the MnN_6 coordination has high bond distortion but lower angular distortion in the LS state (5 K) compared to the HS state at 200 K, i.e., far away from the transition. Trigonal compression in the LS state dominates over the twisting distortion, which is the primary distortion factor in the HS state, accompanied by the dynamic J-T effect.

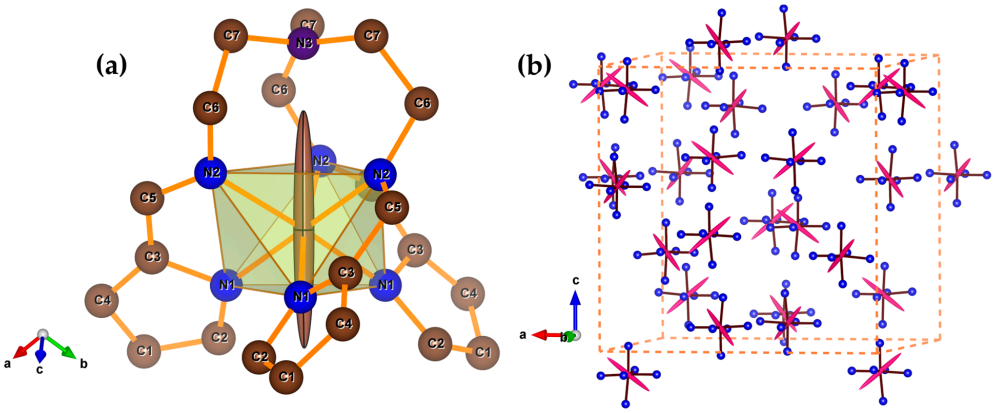

Figure 1. (**a**) Anisotropy ellipsoid obtained from the susceptibility tensor at 5 K overlaid on the molecule (without hydrogen bond). The strong axiality of the ellipsoid indicates that the easy axis of magnetization is along the molecular C_3 symmetry axis, which lies along four local <111> directions, as shown with reference to the crystallographic axes. (**b**) The anisotropy ellipsoid (pink) is plotted over Mn-N (blue dots) coordination polyhedra for the entire unit cell. The overall unit cell remains isotropic with respect to the plotted reference of the crystallographic axes.

At 44 K (LS state), i.e., just below the spin-transition temperature [18], χ_{11} = 0.0533(64) $\mu_B T^{-1}$ and χ_{12} = 0.037(19) $\mu_B T^{-1}$; $\chi_{\parallel}$ and $\chi_{\perp}$ are 0.1237(66) $\mu_B T^{-1}$ and 0.016(66) $\mu_B T^{-1}$, respectively. The ratio $(\frac{\chi_{\parallel}}{\chi_{\perp}})$ = 7.73(96) signifies an Ising-type axiality at 44 K, similar in nature to that at 5 K (Figure 2a). The calculated distortion parameters are ζ = 0.412 Å, Σ = 60.094°, and Θ = 196.97° with an average Mn-N bond length of 2.026 Å and a unit cell parameter a = 19.851 Å. In the HS state at 50 K, just above the transition, the refinement results are χ_{11} = 0.0840(50) $\mu_B T^{-1}$, χ_{12} = 0.014(16) $\mu_B T^{-1}$. Corresponding $\chi_{\parallel}$ and $\chi_{\perp}$ values are 0.112(52) $\mu_B T^{-1}$ and 0.07(52) $\mu_B T^{-1}$, respectively. The ratio $(\frac{\chi_{\parallel}}{\chi_{\perp}})$ = 1.6(14) suggests the evolution of the "needle shape" in the LS state into a "weakly prolate-type" anisotropy above the transition (Figure 2b). The unit cell parameter at 50 K is 19.965(15) Å. The average Mn-N bond length is 2.128 Å, and the distortion parameters are ζ = 0.363 Å, Σ = 71.558°, and Θ = 233.429°. The net contraction of the unit cell volume is 135.545 $Å^3$ (1.7%) when the temperature changes from 50 K to 44 K. With a temperature variation of only 6 K, the change in the average Mn-N bond is 4.79%, and the change in distortion parameters ζ, Σ and Θ are 11.89%, 16.02%, and 15.62%, respectively. The volumetric change and distortion are much more important due to the spin transition than the usual consequence of temperature changes in the 5 K–44 K and 50 K–200 K ranges, as found in single-crystal X-ray diffraction [14].

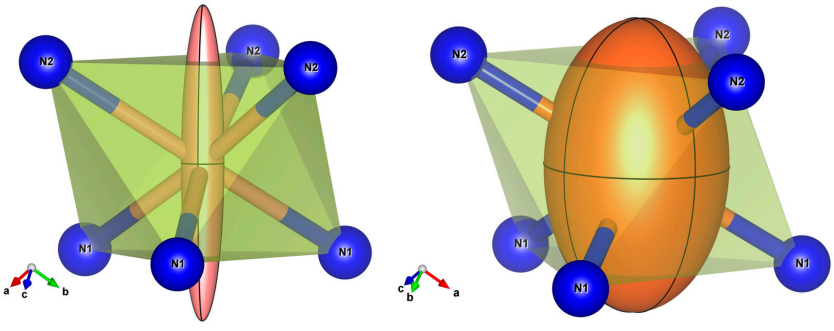

(a) 44 K : $m_{\parallel}$ = 0.68 μ_B
$m_{\perp}$ = 0.09 μ_B

(b) 50 K : $m_{\parallel}$ = 0.62 μ_B
$m_{\perp}$ = 0.39 μ_B

Figure 2. Shape of anisotropy ellipsoid in the vicinity of spin transition: (**a**) Ising-type at 44 K and (**b**) weakly prolate-type of anisotropy ellipsoid at 50 K overlaid on Mn-N coordination polyhedral with moment parallel to the C_3 axis, i.e., along <111> direction and perpendicular components which lie in the (111) plane at each temperature.

https://doi.org/10.3390/magnetochemistry12050056

In the hysteresis loop between 50 K and 44 K, signatures of phase coexistence and irreversibility appear through the evolution of the diffraction peaks exhibiting a "shoulder-like" shape in some peaks (Figure 3a). The system possesses cubic symmetry in the full temperature range of 5–200 K, and important changes in atomic positions occur during the abrupt spin transition. Therefore, for a qualitative understanding of anisotropy and spin state phases, the refinement of the patterns at intermediate phases through the transition is carried out considering the possibility of coexistence of HS and LS states close to the transition temperature, but in the absence of a structural transition [24]. Best fitting (Suppl. Figures S6 and S7) is achieved by incorporating two phases with the unit cell parameters and atomic positions of the HS phase at 50 K and the LS phase at 44 K, as mentioned earlier, rather than a single phase. The refinement is carried out by setting all other parameters fixed and verifying only the scale factors, χ_{11} and χ_{12}, of the two phases. The contribution (in weight percentage) of each phase is calculated as $W_i = \frac{Scale_i}{\sum Scale_i}$, where i corresponds to HS and LS populations. It clearly shows hysteretic temperature variation (Figure 3b). The average magnetic moment per Mn^{3+} of the system in such a mixed state is calculated using the contribution of each phase as $< m > = W_{HS} * \mathrm{m(HS)} + W_{LS} * \mathrm{m(LS)}$. The hysteretic nature of temperature variation in weight percentage of HS (W_{HS}%) and LS (W_{LS}%) and the average magnetic moment (Figure 3c) per Mn^{3+} are reminiscent of the irreversibility of the spin transition observed in macroscopic magnetization [11,17]. It is worth noting that the aforementioned values may slightly vary with the measurement resolution, rate of temperature variation, and sample type (powder and single crystal). However, this analysis undoubtedly indicates the presence of mixed spin states in the intermediate-temperature regime. The hysteretic nature of the spin-transition and the phase coexistence signify a complex transition process related to the growth, nucleation, and propagation mechanisms of HS and LS domains one over the other during the transition [5,24–27].

In the HS state, the anisotropy has a significant perpendicular component, which leads to a deviation from needle-like Ising-type anisotropy toward a weakly prolate-type anisotropy, although the easiest axis of magnetization lies along the C_3 axis. This is consistent with previous INS (D = -5.73 cm^{-1} and E = $|0.475|$ cm^{-1}) [18] and EPR (D = -5.88 cm^{-1} and E = $|0.50|$ cm^{-1}) [17] studies, which proposed an effective axial anisotropy along the C_3 axis. However, the presence of a significant perpendicular component, thus a weakly prolate-type anisotropy ellipsoid with a low ratio, aligns the magnetic moment perpendicular to the C_3 axis, as shown by the PNPD data. Therefore, it provides a pathway for magnetoelectric coupling to tune electric dipole polarization due to J-T distortion (along N1-Mn-N2) by applying a magnetic field perpendicular to the C_3 axis [11,18,19]. In the LS state, the INS study proposed a large positive single-ion anisotropy (D = +39 cm^{-1}) without any rhombic term (E = 0) in the Hamiltonian. In Ref. [18], the authors considered two possibilities, a positive or negative uniaxial trigonal distortion parameter Δ to account for the INS transition peak observed at 4.87 meV (namely $\Delta = -1100$ cm^{-1} or $\Delta = +800$ cm^{-1}). In their model, D is related to the energy gap $\delta E \approx \phi(\kappa\lambda)^2/|\Delta|$, where ϕ = 1 (Δ negative) or ϕ = 2 (Δ positive), κ is the orbital reduction factor (close to 1), and λ is the spin–orbit coupling (estimated at -180 cm^{-1}). The sign of Δ, and thus of D, is therefore not directly attainable with INS, and it was conjectured that one scenario was more plausible than the other with no definitive proof. The PNPD analysis in the LS state suggests a strong needle-shaped Ising anisotropy oriented along the C_3 axis with a very large ratio. This strong axial nature of anisotropy in the LS state appears to be contradictory to the then-proposed large positive D value.

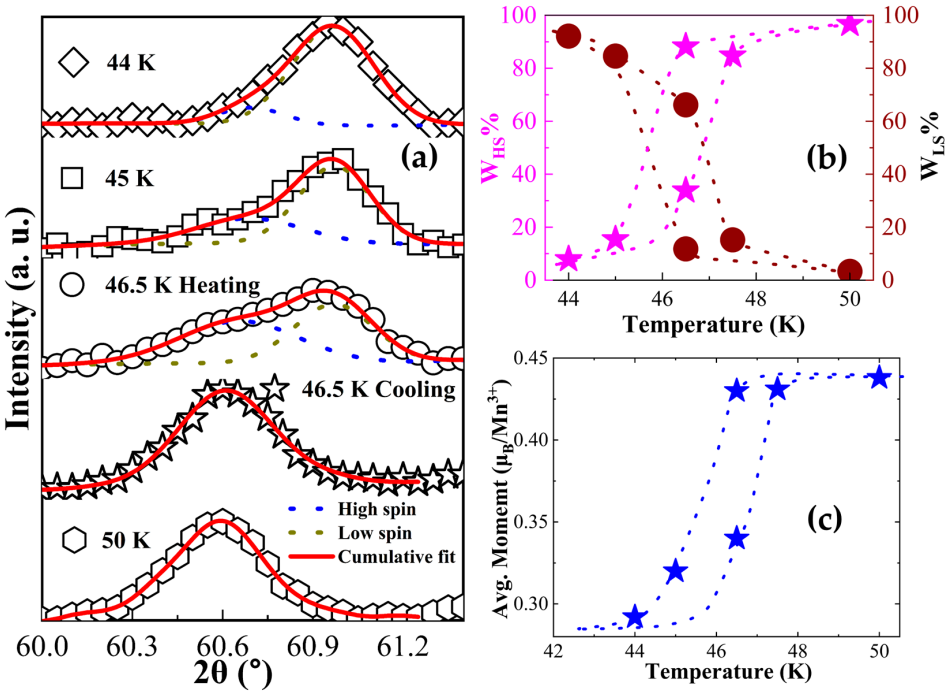

Figure 3. (**a**) Thermal irreversibility and broadening of one of the reference Bragg peaks (6 5 3) in the intermediate temperature regime during transition at 44 K, 45 K, 46.5 K (cooling and heating), and 50 K. Mn^{3+}. (**b**) The weight percentage of HS (left vertical scale) and LS (right vertical scale) contributions obtained from the scale factor. (**c**) Irreversible hysteretic temperature variation in the average magnetic moment per Mn^{3+}. In panel (a), the Gaussian fitting of the peak at different temperatures implies the presence of different contributions in the intermediate-temperature regime. In panel (b) The weight percentage corresponding to HS contribution (W_{HS}%) and LS contribution (W_{LS}%) is obtained from the Rietveld refined scale factor $W_i = \frac{Scale_i}{\sum Scale_i}$, where i = HS, LS.In panel (**c**) the irreversible hysteretic temperature variation in the average magnetic moment $< m > = W_{HS} * \mathrm{m(HS)} + W_{LS} * \mathrm{m(LS)}$ per Mn^{3+} is calculated considering the contribution from each phase. The magnetic moment contributions, m(HS) and m(LS), are obtained from the Rietveld refinement of the PNPD data (fitting and corresponding reliability parameters are reported in the Supplementary Information).

4. Conclusions

In conclusion, the magnetic anisotropy of the $[Mn^{III}(pyrol)_3(tren)]$ in HS and LS states has been determined by PNPD. The analysis suggests a weakly prolate-type magnetic anisotropy, with the easiest direction of the magnetization lying along the threefold C_3 axis and the perpendicular direction. The ratio ($\frac{\chi_\parallel}{\chi_\perp} = 1.60(14)$) of the components of the parallel and perpendicular to the C_3 axis at 50 K suggest that the large magnetic moment can be induced along the perpendicular direction. The anisotropy in the HS state is consistent with the rhombic term in the INS study and the report of tunability of ME coupling by applying a magnetic field along the (110) direction. In the LS state, needle-shaped Ising-type anisotropy is obtained with a relatively high parallel to perpendicular component ratio ($\frac{\chi_\parallel}{\chi_\perp} = 9.29(24)$) at 5 K. The strong axial anisotropy in the LS state seemingly challenges the scenario of a positive uniaxial parameter D = +39 cm^{-1} inferred from INS as one of two plausible solutions [18]. Even though high magnetic anisotropy is observed as a result of distortion and spin–orbit coupling, the overall system remains isotropic with respect to the crystal axes, respecting the cubic symmetry of the crystal. The analysis in the vicinity of and through the transition reveals the irreversible coexistence of both HS and LS states, most probably in the form of domains (nucleation and growth driven by temperature). In this regard, key complementary information could be obtained

by performing high-resolution INS inside the hysteresis loop of the spin transition to better characterize the mixed-spin state, thus addressing the remaining issues in this archetypical thermal spin-transition material.

Supplementary Materials: The following supporting information can be downloaded at: https://www.mdpi.com/article/10.3390/magnetochemistry12050056/s1, Figure S1: Rietveld refinement of the flipping sum ($I_+ + I_-$) at 200 K and the flipping difference ($I_+ - I_-$) pattern at 200 K. Figure S2. Average structure of MnN_6 polyhedra under dynamic Jahn-Teller distortion at 200 K and threefold C_3 axis along [111] direction; Figure S3. Rietveld refinement of the (a) flipping sum ($I_+ + I_-$), (b) and difference ($I_+ - I_-$) pattern at 5 K. Figure S4. Rietveld refinement of the (a) flipping sum ($I_+ + I_-$) and (b) difference ($I_+ - I_-$) pattern at 50 K. Figure S5. Rietveld refinement of the (a) flipping sum ($I_+ + I_-$) and (b) difference ($I_+ - I_-$) pattern at 44 K. Figure S6. Rietveld refinement of flipping sum (a–f) at different fixed temperatures in the intermediate temperatures 44 K–50 K during transition, considering phase coexistence of HS and low spin. Figure S7. Rietveld refinement of flipping difference (a–e) at different fixed temperatures in the intermediate temperatures 44 K–50 K during transition, considering phase coexistence of HS and low spin. Figure S8. Susceptibility curve of the title compound represented as χT product versus temperature obtained at 0.05 T during cooling and warming. Table S1: Acquisition times of the Polarized Neutron Diffraction patterns obtained on D20 for the data taken under a magnetic field of 5.5 Tesla and various temperatures (5 K–200 K).

Author Contributions: Y.G. prepared the reported compound. I.K., A.G., T.C.H., E.L.-B., and G.C. performed the Polarized Neutron Diffraction experiment. P.P., I.K., A.G., and G.C. analyzed the data and contributed to the interpretation and modeling. P.P. and G.C. wrote the paper and integrated contributions from co-authors. G.C. supervised the project and acquired the funding. All authors have read and agreed to the published version of the manuscript.

Funding: This research was partially funded by the APICONE funding scheme of CEA and CNRS with the grant name PODIMAG as well as by the Fonds de la Recherche Scientifique-FNRS (PDR T.0095.21).

Institutional Review Board Statement: Not applicable.

Informed Consent Statement: Not applicable.

Data Availability Statement: The neutron raw data measured on the D20 diffractometer are available upon request.

Acknowledgments: The authors are thankful to the ILL technical staff for their support and help during the neutron diffraction experiment.

Conflicts of Interest: The authors declare no conflict of interest.

References

1. Chilton, N.F. Molecular Magnetism. *Annu. Rev. Mater. Res.* **2022**, *52*, 79–101. [CrossRef]
2. Moreno-Pineda, E.; Wernsdorfer, W.; Moreno-Pineda, E.; Wernsdorfer, W. Magnetic Molecules as Building Blocks for Quantum Technologies. *Adv. Quantum Technol.* **2025**, *8*, 2300367–2300381. [CrossRef]
3. Roy, S.; Riminucci, A. Perspectives on Molecular Spin-Based Memories. *APL Mater.* **2025**, *13*, 70901–70914. [CrossRef]
4. Vaganov, M.V.; Suaud, N.; Lambert, F.; Cahier, B.; Herrero, C.; Guillot, R.; Barra, A.L.; Guihéry, N.; Mallah, T.; Ardavan, A.; et al. Chemical Tuning of Quantum Spin–Electric Coupling in Molecular Magnets. *Nat. Chem.* **2025**, *17*, 1903–1909. [CrossRef]
5. Ridier, K.; Molnár, G.; Salmon, L.; Nicolazzi, W.; Bousseksou, A. Hysteresis, Nucleation and Growth Phenomena in Spin-Crossover Solids. *Solid State Sci.* **2017**, *74*, A1–A22. [CrossRef]
6. Gukasov, A.; Brown, P.J. Determination of Atomic Site Susceptibility Tensors from Polarized Neutron Diffraction Data. *J. Phys. Condens. Matter* **2002**, *14*, 8831–8839. [CrossRef]
7. Luneau, D.; Gillon, B. Polarized Neutron Diffraction: An Excellent Tool to Evidence the Magnetic Anisotropy—Structural Relationships in Molecules. *Magnetochemistry* **2021**, *7*, 158. [CrossRef]
8. Gukasov, A.; Brown, P.J. Determination of Atomic Site Susceptibility Tensors from Neutron Diffraction Data on Polycrystalline Samples. *J. Phys. Condens. Matter* **2010**, *22*, 502201–502206. [CrossRef] [PubMed]

9. Kibalin, I.A.; Gukasov, A. Local Magnetic Anisotropy by Polarized Neutron Powder Diffraction: Application of Magnetically Induced Preferred Crystallite Orientation. *Phys. Rev. Res.* **2019**, *1*, 033100–033108. [CrossRef]
10. Sim, P.G.; Sinn, E. First Manganese(III) Spin Crossover and First D4 Crossover. Comment on Cytochrome Oxidase. *J. Am. Chem. Soc.* **1981**, *103*, 241–243. [CrossRef]
11. Garcia, Y.; Kahn, O.; Ader, J.P.; Buzdin, A.; Meurdesoif, Y.; Guillot, M. The Effect of a Magnetic Field on the Inversion Temperature of a Spin Crossover Compound Revisited. *Phys. Lett. A* **2000**, *271*, 145–154. [CrossRef]
12. Nakano, M.; Matsubayashi, G.-E.; Matsuo, T. Dielectric Behavior of Manganese(III) Spin-Crossover Complex [Mn(Taa)]. *Phys. Rev. B—Condens. Matter Mater. Phys.* **2002**, *66*, 21412–21414. [CrossRef]
13. Sawada, Y.; Kimura, S.; Watanabe, K.; Nakano, M. High-Field Optical Spectroscopy of the Spin-Crossover Complex [Mn III(Taa)]. *J. Low Temp. Phys.* **2013**, *170*, 424–429. [CrossRef]
14. Guionneau, P.; Marchivie, M.; Garcia, Y.; Howard, J.A.K.; Chasseau, D. Spin Crossover in [MnIII(Pyrol)3(Tren)] Probed by High-Pressure and Low-Temperature x-Ray Diffraction. *Phys. Rev. B* **2005**, *72*, 214408–214415. [CrossRef]
15. Garcia, Y.; Paulsen, H.; Schünemann, V.; Trautwein, A.X.; Wolny, J.A. Estimate of the Vibrational Contribution to the Entropy Change Associated with the Spin Transition in the D4 Systems [MnIII(Pyrol)3tren] and [CrII(Depe)2I2]. *Phys. Chem. Chem. Phys.* **2007**, *9*, 1194–1201. [CrossRef] [PubMed]
16. Yu, J.X.; Chen, D.T.; Gu, J.; Chen, J.; Jiang, J.; Zhang, L.; Yu, Y.; Zhang, X.G.; Zapf, V.S.; Cheng, H.P. Three Jahn-Teller States of Matter in Spin-Crossover System Mn(Taa). *Phys. Rev. Lett.* **2020**, *124*, 227201–227206. [CrossRef]
17. Kimura, S.; Hagiwara, M.; Narumi, Y.; Nakano, M.; Kindo, K. High Frequency ESR Measurements on the Spin Crossover Complex [Mn III(Taa)]. *J. Phys. Conf. Ser.* **2010**, *200*, 022025. [CrossRef]
18. Ridier, K.; Petit, S.; Gillon, B.; Chaboussant, G.; Safin, D.A.; Garcia, Y. Magnetic Neutron Spectroscopy of a Spin-Transition Mn^{3+} Molecular Complex. *Phys. Rev. B* **2014**, *90*, 104407–104413. [CrossRef]
19. Chikara, S.; Gu, J.; Zhang, X.G.; Cheng, H.P.; Smythe, N.; Singleton, J.; Scott, B.; Krenkel, E.; Eckert, J.; Zapf, V.S. Magnetoelectric Behavior via a Spin State Transition. *Nat. Commun.* **2019**, *10*, 4043. [CrossRef]
20. Otsuki, Y.; Kimura, S.; Awaji, S.; Nakano, M. Enhancement of the Magnetoelectric Effect Using the Dynamic Jahn-Teller Effect in a Transition-Metal Complex. *Phys. Rev. Lett.* **2022**, *128*, 117601–117606. [CrossRef]
21. Hansen, T.C.; Henry, P.F.; Fischer, H.E.; Torregrossa, J.; Convert, P. The D20 Instrument at the ILL: A Versatile High-Intensity Two-Axis Neutron Diffractometer. *Meas. Sci. Technol.* **2008**, *19*, 034001. [CrossRef]
22. Lelièvre-Berna, E.; Wills, A.S.; Bourgeat-Lami, E.; Dee, A.; Hansen, T.; Henry, P.F.; Poole, A.; Thomas, M.; Tonon, X.; Torregrossa, J.; et al. Powder Diffraction with Spin Polarized Neutrons. *Meas. Sci. Technol.* **2010**, *21*, 055106. [CrossRef]
23. Ketkaew, R.; Tantirungrotechai, Y.; Harding, P.; Chastanet, G.; Guionneau, P.; Marchivie, M.; Harding, D.J. OctaDist: A Tool for Calculating Distortion Parameters in Spin Crossover and Coordination Complexes. *Dalt. Trans.* **2021**, *50*, 1086–1096. [CrossRef] [PubMed]
24. Pillet, S.; Hubsch, J.; Lecomte, C. Single Crystal Diffraction Analysis of the Thermal Spin Conversion in [Fe(Btr)2(NCS)2](H2O): Evidence for Spin-like Domain Formation. *Eur. Phys. J. B—Condens. Matter Complex Syst.* **2004**, *38*, 541–552. [CrossRef]
25. Fourati, H.; Boukheddaden, K. Experimental Evidence for the Elastic Long-Range Character of the Spin Crossover Transition in Cooperative Single Crystals. *Phys. Rev. B* **2020**, *101*, 224101–224113. [CrossRef]
26. Slimani, A.; Boukheddaden, K.; Yamashita, K. Effect of Intermolecular Interactions on the Nucleation, Growth, and Propagation of like-Spin Domains in Spin-Crossover Materials. *Phys. Rev. B* **2015**, *92*, 014111–014120. [CrossRef]
27. Shahed, H.; Sharma, N.; Angst, M.; Voigt, J.; Perßon, J.; Prakash, P.; Törnroos, K.W.; Chernyshov, D.; Gildenast, H.; Ohl, M.; et al. Structural Insight into the Cooperativity of Spin Crossover Compounds. *Acta Crystallogr. Sect. B Struct. Sci. Cryst. Eng. Mater.* **2023**, *79*, 354–367. [CrossRef] [PubMed]